Global electromagnetic gyrofluid/gyrokinetic computation of turbulence and self consistent rotation in large tokamaks

B. D. Scott[1], A. Bottino[1], R. Hatzky[1b], S. Jolliet[2],
A. Kendl[3], B. F. Mcmillan[2], D. Reiser[4], T. Ribeiro[5]

[1]Max-Planck-Institut für Plasmaphysik, EURATOM Association, D-85748 Garching
[1b]Rechenzentrum der Max-Planck-Gesellschaft, Garching, Germany
[2]Centre de Recherches en Physique des Plasmas, EPFL, Lausanne, Switzerland
[3]Inst fuer theor Physik, Euratom/OeAW, University of Innsbruck, Innsbruck, Austria
[4]Institut fuer Plasmaphysik, FZ-Juelich, Euratom, Juelich, Germany
[5]Instituto de Plasmas e Fusão Nuclear, Euratom, Lisbon, Portugal
e-mail: bruce.scott@ipp.mpg.de

Abstract. We report on gyrofluid and gyrokinetic numerical studies of edge and core turbulence in tokamak geometry, with emphasis on the self consistent interaction with the equilibrium. Gyrokinetic PIC and Vlasov as well as gyrofluid models are given and used in the analysis. Selected nonlinear results on tokamak rotation and edge turbulence are given.

1. Global Electromagnetic Gyrokinetic Computation

The gyrokinetic particle in cell (PIC) code ORB5 [1] has been extended to kinetic electron parallel responses. Although based on delta-f techniques, it actually solves a variant of the total-f gyrokinetic equations. The particle Lagrangian and Hamiltonian are

$$L_p = \left[\frac{e}{c}\mathbf{A} + mv_\parallel \mathbf{b}\right]\cdot\dot{\mathbf{R}} + \frac{mc}{e}\mu\dot{\vartheta} - H \qquad\qquad H = \frac{m}{2}v_\parallel^2 + \mu B + eJ_0\phi \tag{1}$$

where J_0 is an orbit averaging operator implemented through sampling over cubic spline basis functions. The particle coordinates are $\mathbf{Z}_p \in \{\mathbf{R}, v_\parallel, \mu, \vartheta\}$ giving the spatial position of the gyrocenter, and velocity space coordinates describing the parallel velocity, magnetic moment, and gyroangle. The particles are actually markers through which the distribution function f is solved for via characteristics [2]. f is given by

$$f = F^M + \delta f \qquad\qquad \delta f = \sum_p w_p \oint \frac{d\vartheta}{2\pi}\delta^6(\mathbf{z} - \mathbf{Z}_p - \mathbf{a}_L) \tag{2}$$

where F^M is a prescribed function of the constants of the motion and w_p is the weight associated with the p-th marker and $\mathbf{Z}_p$ the position of the gyrocenter. The integral over ϑ reflects representation of the particle as a charged ring of radius ρ_L, with the directed gyroradius $\mathbf{a}_L$ averaging over the fast gyromotion. The Lagrangian for the entire system including the field potential ϕ is given by

$$L = \sum_{\mathrm{sp}} \int d\Lambda\, f L_p + \int dV \frac{n_0 M_i c^2}{2B^2}\left|\nabla_\perp \phi\right|^2 \tag{3}$$

with the sum over species and the integrals over phase space and the spatial domain, respectively, and n_0 a prescribed density profile controlling the strength of the polarisation density. The expression of this latter as a field energy corresponds to the use of the first order gyrokinetic Hamiltonian — the second order screening terms of Ref. [3] are approximated by this field energy term. Full energetic consistency is retained by making this approximation in the

Lagrangian and then keeping the resulting Euler-Lagrange equations intact [4]. The Euler-Lagrange equations are given by

$$B_{\|}^{*}\dot{\mathbf{R}} = \nabla H \cdot \frac{c}{e}\frac{\mathbf{F}}{B} + v_{\|}\mathbf{B}^{*} \qquad B_{\|}^{*}(m\dot{v}_{\|}) = -\mathbf{B}^{*}\cdot\nabla H \qquad \dot{\mu} = 0 \tag{4}$$

for the particle coordinates, where the auxiliary quantities are defined as

$$\mathbf{F} = \varepsilon\cdot\mathbf{B} \qquad \mathbf{B}^{*} = \mathbf{B} - \nabla\cdot m v_{\|}\frac{c}{e}\frac{\mathbf{F}}{B} \qquad B_{\|}^{*} = B^{-1}\mathbf{B}\cdot\mathbf{B}^{*} \tag{5}$$

with ε the 3D Levi-Civita tensor; hence $\mathbf{F}$ is the space-space part of the Maxwell field tensor. For the field potential, variation $\delta L/\delta\phi$ finds

$$\nabla\cdot\frac{n_0 M_i c^2}{B^2}\nabla_{\perp}\phi + \sum_{\mathrm{sp}}\int dW\, eJ_0\delta f = 0 \tag{6}$$

where the integral is over velocity space and the same J_0 operator averaging the spatially dependent potential onto gyrocenters now acts to place the gyrocenters in space. This equation represents quasineutrality since the field term $E^2/8\pi$ is neglected against the E-cross-B (ExB) energy due to $v_A^2 \ll c^2$ being well satisfied (i.e., the Alfvén velocity is deeply subrelativistic).

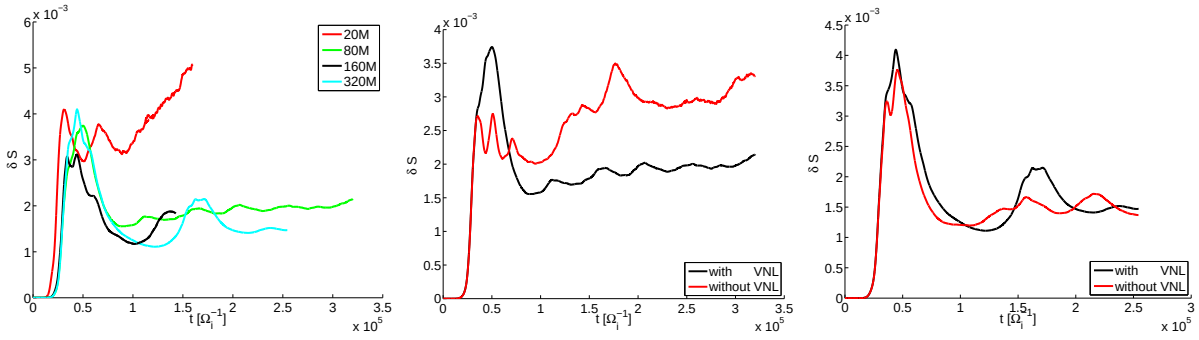

FIG. 1: Examples of the effects of resolution in ORB5 computations (see text).

In ORB5 the particle loading is according to the energy, magnetic moment, and the canonical toroidal momentum (in lieu of the minor radius coordinate). This minimises the size of initial transients in the axisymmetric responses and enters because δf includes the structure of the background density and temperature profiles. A common issue is the presence or absence of the parallel velocity nonlinearity; this is kept in the contribution due to $eJ_0\phi$ to H in the equation for $(m\dot{v}_{\|})$. Without this term one does not even have phase space conservation because the $\mathbf{B}^{*}$ terms in Eqs. (4) would no longer form a bracket substructure. However, the effect has been found in ORB5 to be negligible, indeed small by one order in $\rho_{*} = \rho_s/a$ where $\rho_s = c_s/\Omega_i$ is the ion sound gyroradius with acoustic speed c_s and ion gyrofrequency Ω_i. This as well is a resolution test: with 80M markers in a standard case (ion temperature gradient (ITG) turbulence "global Cyclone" case detailed in Ref. [5]) with $\rho_{*} = 1/184$ switching the nonlinearity in and out made a difference of about 50% in the delta-f entropy $S = \sum_p w_p^2$ while in the same case with 320M markers differences were within the temporal fluctuations in S. With the nonlinearity the two cases were nearly convergent (Fig. 1, center and right frames).

1.1. noise and noise control

The issue of noise in PIC methods has been raised repeatedly as a statistical issue. Equivalently, however, it is a matter of resolution, with the number of particles per active wavenumber serving in a similar way as the resolution on the velocity space grid in a Vlasov ("continuum") computation. If this is insufficient then it is impossible to describe structures involving higher moments, and the issue enters with such gravity because the usual situation is of drive by temperature gradients. An example for the above ITG case is shown in Fig. 1 (left frame). A systematic study has been carried out in ORB5 concerning this within simplified "ETG" computations (defined by expressing δf as particle weights for only one species and setting the other in simple proportionality to ϕ without splitting off the flux surface average). It is found that the problems usually attributable to noise — a strong decrease in the transport and increase in the δf entropy S with increasing time — actually result from this insufficient resolution, in agreement with previous studies using Vlasov methods in which noise is not an issue [6]. The signal to noise (S/N) ratio diagnostic in ORB5 is a measure of the ratio of delta-f entropy content in a band of higher values of $k_{\|}qR = (m - nq)$ to the content in the band with roughly ± 5. The S/N is above 50 in saturation but drops sharply as the free energy spectrum spreads out. Higher numbers of particles are found to delay this drop but never prevent it.

In ORB5 a method has been found to counter this effect and allow for essentially indefinite turbulence saturation similar to fluid and Vlasov models (which necessarily contain numerical dissipation to contain the cascades [7–10]). Krommes suggested using a simple Krook operator to provide dissipation [11]. While this acts everywhere in the spectrum, the hope was that it would indirectly act preferentially on short wavelengths where the tendency to develop larger values of w_p^2 is greatest (the free energy cascade in δf is always powerful and direct — more on this below). This method was developed more generally to conserve an arbitrary set of moments, most specifically ExB flow energy [12]. It appears to have solved much of the noise and saturation problem — ETG and ITG turbulence runs with relaxing profiles have been carried out for as long as $1700a/c_s$, with the S/N dropping from about 45 to 35 over the range beyond $200a/c_s$. The slow decay follows slow relaxation of the profile, as with the value $\rho_* = 1/184$ the turbulence/transport scale separation is well achieved.

1.2. global studies of plasma rotation

The plasma experiences poloidal rotation as the potential dynamically builds up layers which have solely radial dependence. On small scales (about 10 to $20\rho_s$) this is a fluctuating component which is forced at all frequencies by the turbulence but responds resonantly at the geodesic oscillation frequency in addition to a component which have zero frequency. Nomenclature varies, but these can be referred to as geodesic oscillations and zonal flows, respectively ("zonal" $\leftrightarrow$ flux surface average). They represent eigenmodes of the system whose ratio given an initial perturbation with purely zonal dependence of δf hence ϕ forms a standard test [13]. However, the issue of wider interest to tokamak phenomenology is the extent to which the large-scale zonal potential and the ExB rotation that represents can be caused by turbulent or by equilibrium processes. In the absence of turbulence or other dynamics the $\sin\theta$ and $\cos\theta$ axisymmetric sideband components are such that flows are divergence free and parallel forces are in balance. This is the essential assumption behind neoclassical theory and therefore one would expect rotation to be neoclassical [14]. However, there are indications that this might not be the case [15].

Investigation of this using ORB5 is beginning. In the meantime study of it has been carried out using the global gyrofluid model GEM [16]. Global core models are defined by choosing a set

of tokamak core representative parameters and simulating the region typically $0.2 < r/a < 1.0$ using a global field aligned coordinate system [17] in which the large-scale MHD component determines the Shafranov shift and Pfirsch-Schlüter current self consistently [18]. Broadband fluctuations are initialised and the entire system is allowed to relax — no sources are applied, a sink at $r = a$ keeps the dependent variables at zero thereby removing fluctuation energy [19], and the turbulence is driven by conservative transfer out of the axisymmetric component into the eddy components. Even with $\rho_* = 1/200$ the relaxation of the profiles is below ten percent over the run length of $800a/c_s$. Cases with ρ_*^{-1} varying from 50 to 800 (ITER scale) in successive steps of factors of two were taken.

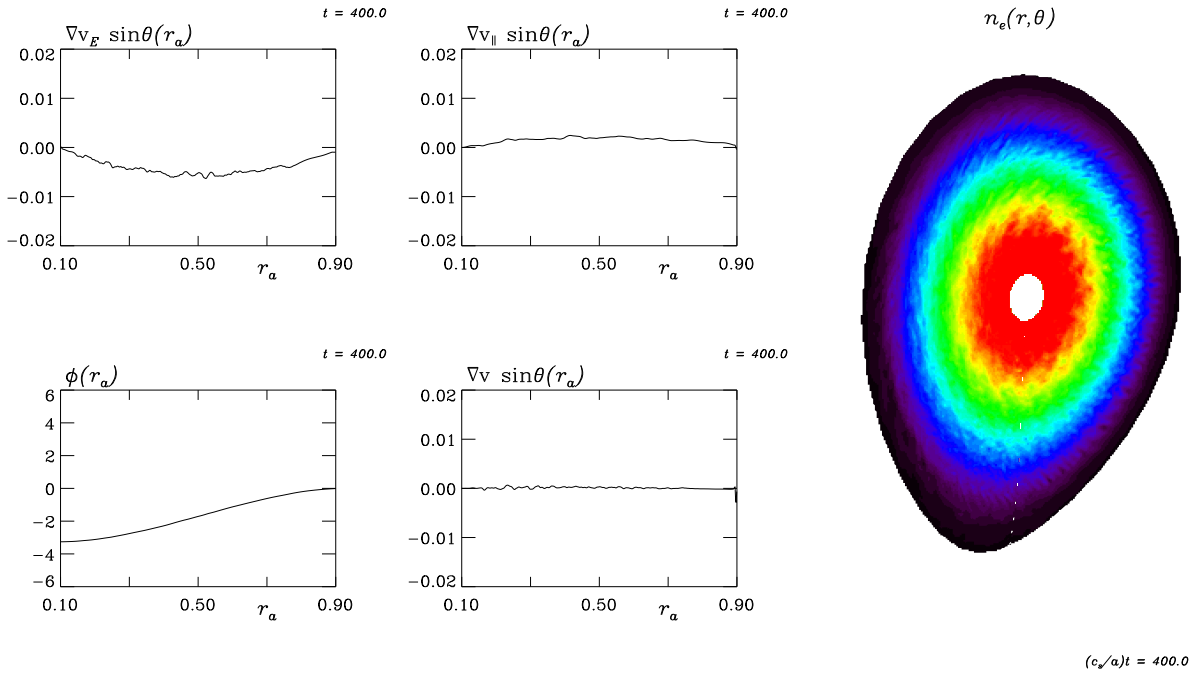

FIG. 2: Flow profile results in GEM for a shaped tokamak case with $\rho_* = 1/200$ *(see text).*

Flows are diagnosed via the $\sin\theta$ component of the divergences in the ion gyrocenter continuity equation [18]. If the linear (parallel, magnetic drift, E-cross-B) compression terms are in balance then equilibrium ("neoclassical") processes control the flows as turbulence is a small correction. Turbulence forcing scales as ρ_*^2 while the equilibrium divergences scale as ρ_* simply. The GEM results find that the neoclassical processes become more dominant the larger the tokamak, with the crossover regime near $\rho_*^{-1} = 200$ for smooth profiles or about 400 for profiles with detailed structure. For large tokamaks zonal flow generation is too weak by comparison to play a central role. For finite beta they are weakened still. A representative result for a shaped case with $\rho_*^{-1} = 200$ representative of present day medium size tokamaks is given in Fig. 2. The finite ExB profile divergence (v_E) resulting from the profile $\phi(r_a)$, and its compensation by the toroidal drift and parallel flow ($v_\parallel$) divergences is shown by the near-zero total divergence (v). The electron density variation on which the fluctuations are still visible is shown in the right frame. The turbulent zonal flows are barely visible as unsteadiness on the otherwise smooth profile of the ExB divergence. For $\rho_*^{-1} = 400$ and larger the zonal flow component is no longer visible. This indicates unlikelihood that turbulence can determine the ExB rotation profile on large radial scales. However, the moment variable closure in the model is necssarily dissipative (otherwise, no reasonable neoclassical equilibrium is found). The result remains open to

criticism on these grounds. Investigation with ORB5 has a prerequisite that the neoclassical equilbirium should be found before investigation is done with the turbulence. At the time of this writing investigation is ongoing, with demonstration of a neoclassical rotation profile only just achieved. A result on the rotation profile in the presence of turbulence using the sideband divergence diagnostic on long-term saturated should emerge in the coming months.

2. Gyrokinetic Theory and Global Total-f Computation

The Lagrangian field theory method underlying the ORB5 model ultimately rests on the Lagrangian/Hamiltonian field theory of gyrokinetics by which the particle Lagrangian in electrostatic [3] or electromagnetic [20] form is placed within the structure of a total Lagrangian for the particle/field system [21,4,22]. Computations usually require an approximated version of this to be made tractable, but as long as this is undertaken at the level of the particle/field Lagrangian, the basic consistency of the theory is guaranteed. Indeed, this is behind the basic proof of energy conservation in the ORB5 model whose predecessor was given in Ref. [23]. The linearisation of the polarisation by the electrostatic models is an example of how to do this properly. For edge turbulence and overall dynamics, however, the scale separation is more marginal and indeed for such events as large scale MHD phenomena it is absent. If the background density is to be allowed to change significantly (i.e., build a pedestal or suffer a gradient collapse) then the polarisation must be nonlinear. Moreover, edge turbulence is fundamentally electromagnetic [24,25].

With this in mind the electromagnetic Lagrangian in the parallel canonical momentum formulation of Ref. [20] is taken as a starting point and the model formulated as a field theory following the methods cited above. The model is called FEFI (full electrons, full ions) and represents a total-f electromagnetic gyrokinetic model which is in principle capable of global simulation. The first version of this concentrates on the ability for the large scale MHD processes to relax toward equilibrium away from which the turbulence always disturbs them. Hence gyroaveraging is neglected and long-wavelength forms are used in the polarisation terms. These restrictions will be relaxed in future work. The Lagrangian is

$$L = \sum_{\mathrm{sp}} \int d\Lambda \left[\left(\frac{e}{c}\mathbf{A} + p_z \mathbf{b} \right) \cdot \dot{\mathbf{R}} + \frac{mc}{e}\dot{\vartheta} - H \right] f - \int dV \, \frac{B_\perp^2}{8\pi} \tag{7}$$

where the Hamiltonian, generalised potential, and squared ExB velocity are

$$H = m\frac{U^2}{2} + \mu B + e\phi_G \qquad \phi_G = \phi - \frac{m}{e}\frac{v_E^2}{2} \qquad v_E^2 = \frac{c^2}{B^2}\left|\nabla_\perp \phi\right|^2 \tag{8}$$

and the parallel velocity functional and perturbed magnetic field strength are given by

$$U = \frac{1}{m}\left(p_z - \frac{e}{c}A_\parallel \right) \qquad B_\perp^2 = \left|\nabla_\perp A_\parallel\right|^2 \tag{9}$$

with dV and dW the space and velocity space volume elements, and $d\Lambda = dV\,dW$ is the phase space volume element. The sum is over species and m and e are the mass and charge of each species. The resulting gyrokinetic equation is

$$B_\parallel^* \frac{\partial f}{\partial t} + \nabla H \cdot \frac{c}{e}\frac{\mathbf{F}}{B} \cdot \nabla f + \mathbf{B}^* \cdot \left(\frac{\partial H}{\partial p_z}\nabla f - \frac{\partial f}{\partial p_z}\nabla H \right) = C(f) \tag{10}$$

where $\mathbf{F} = (\nabla \mathbf{A}) - (\nabla \mathbf{A})^T$ and $\mathbf{B}^* = \mathbf{B} - p_z(c/e)\nabla \cdot (\mathbf{F}/B)$ and $B_\parallel^* = \mathbf{b} \cdot \mathbf{B}^*$. Here we approximate $\mathbf{F} \approx (RB/I)\mathbf{F}_0$ with $I = R_0 B_0$ a constant and $\nabla \cdot \mathbf{F}_0 = 0$, so that $B_\parallel^* = B$. We assume arbitrarily

weak collisionality so that the collision operator C consists of hyperdiffusion in p_z and s (actual collisions are to be implemented later). The spatial coordinates $\{x,y,s\}$ describe a unit-Jacobian Hamada global field-aligned system [17], so that $dV = dxdyds$. The velocity space grid is on $\{p_z,\mu\}$ so that $dW = 2\pi m^{-2}Bdp_z d\mu$. The self consistent field equations resulting from variation of L with respect to ϕ and $A_\parallel$ are

$$\sum_{\rm sp}\int dW\,\left[ef+\nabla\cdot\frac{fmc^2}{B^2}\nabla_\perp\phi\right]=0 \qquad\qquad \nabla_\perp^2 A_\parallel+\frac{4\pi}{c}\sum_{\rm sp}\int dW\,eUf=0 \qquad (11)$$

giving quasineutral polarisation and shear-Alfvén induction, respectively (note here that U in the integral also involves $A_\parallel$).

The list of dependent variables is $f(x,y,s,p_z,\mu)$ and $\phi(x,y,s)$ and $A_\parallel(x,y,s)$, with f advanced in time with Eq. (10) and then ϕ and $A_\parallel$ solved using Eqs. (11). The collisionless part of Eq. (10) is a generalised bracket decomposed into six pieces each computed using the 4th-order Arakawa method. This and the dissipation are combined in a 3rd-order stiffly stable timestep, in a combination known from edge turbulence[26].

The similarity to the ORB5 model should be obvious — the second order term in the FEFI Hamiltonian multiplies the dependent variable f but in ORB5 becomes a field energy term as f is replaced by F^M, kept only for ions and integrated to n_0, and correspondingly the field potential term in polarisation involves n_0 in ORB5 but the entire f in FEFI. In ORB5 the model is electrostatic so that $A_\parallel$ is taken to zero hence $U = p_z/m$ becomes $v_\parallel$. Otherwise, however, the footing they are on is the same: ORB5 uses a delta-f method but is not a delta-f model.

The FEFI code has captured the global Alfvén oscillation, whose dissipation relaxes the parallel current into Pfirsch-Schlüter equilibrium. With the pressure profile contributing to the magnetic drifts, axisymmetric parallel currents result and describe the global geodesic Alfvén oscillation. This damps due to the combination of resistivity and electron Landau damping. The resulting magnetic field is none other than the Shafranov shift. Hence the MHD equilibrium and its disturbance by any present dynamics is computed self consistently. This is a necessary test for any electromagnetic model attempting to simulate edge turbulence with self consistent profiles, not just a gyrokinetic one (for GEM see Fig. 3 of Ref. [18]). Computation of edge turbulence on the entire flux surface has just been done in a case with self consistent sources. The grid was $64\times512\times32$ for the domain $0.85<r/a<0.99$ in (V,ϑ,ξ) coordinates (see Sec. V of Ref. [17]). The velocity space grid was 32×16 for $-5<p_z<5$ and $0<\mu B<10$ in units of $(mT_0)^{1/2}$ and T_0 for each species, respectively, for reference values $T_0=200\,\mathrm{eV}$ and $n_0=2\times10^19\,\mathrm{m}^{-3}$ and $B_0=2.5\,\mathrm{T}$ and $R=3.3a=1.65\,\mathrm{m}$. The actual parameters themselves are results; T for both species varied between 100 and 400 eV and n was between 1 and $3\times10^19\,\mathrm{m}^{-3}$.

3. Gyrokinetic Turbulence Energy Transfer and Saturation

Although the general aim for electromagnetic gyrokinetic is global simulation, it remains useful to study the details of internal processes in a fluxtube model in which the details of energetic consistency are such that the range of control tests one can make is wider (e.g., it is impossible to remove magnetic trapping in FEFI while still keeping the grad-B drift as both arise from the same term in H). By contrast to ORB5 which used a delta-f method, this is actually a delta-f model in which the dynamics is linearised except for the perpendicular nonlinearities entered into by the part of H due to the perturbed fields. The derivation of this delta-FEFI model (and ultimately the best derivation of the GEM model) is given in Ref. [27]. The equations are

$$\frac{\partial\widetilde{g}}{\partial t}+\frac{cF^{xy}}{eB^2}[\widetilde{H},\widetilde{h}]_{xy}+\frac{B^s}{B}[H_0,\widetilde{h}]_{zs}+\mathcal{K}(\widetilde{h})=C(\widetilde{f}) \qquad (12)$$

for $\widetilde{g} = \delta f + (e/T)F^M(v_\parallel/c)A_\parallel$ and $\widetilde{h} = \delta f + (e/T)F^M\phi$ with curvature drifts given by $\mathcal{K} = \nabla(\mu B - mv_\parallel^2 \log R)\cdot(c\mathbf{F}/eB)\cdot\nabla_{\{x,y\}}$ and unperturbed and perturbed Hamiltonian pieces given by $H_0 = mv_\parallel^2/2 + \mu B$ and $\widetilde{H} = eJ_0(\phi - [v_\parallel/c]A_\parallel)$, in which forms the subscripts x and y indicating only those derivatives of the dependent variables are kept while all the geometric information depends only on s in standard fluxtube ordering [28,29,17]. The linearised field equations are

$$\nabla_\perp^2 A_\parallel + \frac{4\pi}{c}\sum_{\rm sp} dW\, ev_\parallel J_0 \widetilde{f} = 0 \qquad\qquad \sum_{\rm sp} dW\left[eJ_0 f + e^2 F^M \frac{J_0^2 - 1}{T}\phi\right] = 0 \qquad (13)$$

and $J_0 = J_0(k_\perp \rho_L)$ is the zeroth Bessel function applied in wavenumber space — x and y may be Fourier transformed since the geometry depends only on s. The collision operator C is a standard pitch angle scattering operator where the electrons are scattered by both species and the ions among themselves. The wavenumber space is $\mathbf{k}_\perp = \{k_x, k_y\}$ with magnitude $k_\perp$.

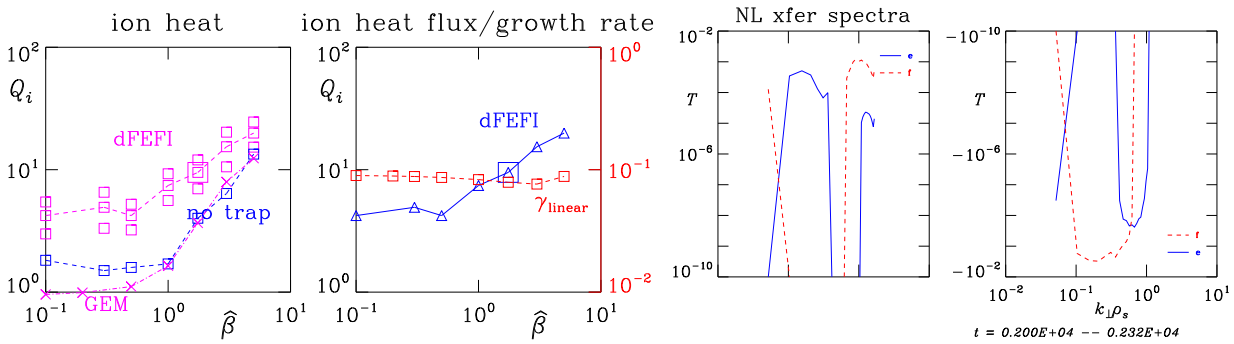

FIG. 3: Beta scaling of the ExB ion heat transport for delta-FEFI, with and without trapping, with comparison to the fluxtube GEM result (leftmost), and with comparison to linear growth rates (left next) Nonlinear energy transfer spectrum in delta-FEFI (right frames), where positive and negative.

This model has been used to explore the general behaviour of edge turbulence as well as cascade dynamics and nonlinear spectral transfer. The transfer function is found by Fourier deomposing each nonlinearity in $\mathbf{k}_\perp$ and contracting with the complex conjugate of either $eJ_0\phi$ or $(T/F^M)\delta f$ and summing over species, for the ExB and thermal free energy transfer functions, respectively. The spectra of these are shown in Fig. 3 (right frames). The results show that the latter is of stronger magnitude by a factor of about 5 and is negative at low-$k_\perp$ and positive with equal total at high-$k_\perp$. The ExB transfer function is of opposite sign everywhere except in the dissipation range $k_\perp\rho_s > 1$. This indicates net energetic input/output which compensates the linear coupling effects (mostly through $J_\parallel$ but also through $\mathcal{K}$ [30]). A strong direct transfer tendency is found for $\sum_{\rm sp}(\delta f)^2(T/2F^M)$ while a subdominant inverst tendency is found for $(1/2)\sum_{\rm sp}(eJ_0\phi)\delta f$, the thermal free energy and ExB energy densities, respectively. The form of this signal is exactly the same as found previously for Hasegawa-Wakatani turbulence [31] and also for the three dimensional fluid models of Refs. [8,30]. The indication is that these transfer tendencies are always present (indeed, in the fluid models the density fluctuation acts as a simplification for δf and the vorticity fluctuation represents $\sum_{\rm sp} e\delta f$). The strength of the nonlinear transfer dynamics is affected by linear dissipative coupling mechanisms, but not its character.

The effect this transfer dynamics has on scaling and turbulence saturation can be found by testing the linear growth rate and mode structure against the fluxes and mode structure of the

fully developed turbulence. The saturation itself is due to the transfer of $(\delta f)^2$ free energy to subgrid scales where it is eliminated by dissipation (see also Figs. 1–3 of Ref. [8] for the fluid model). But the scaling is also strongly affected by the inverse-transfer due to the ExB component. Besides merely shifting the spectrum toward longer wavelength, it also adds to the drive of a mesoscale MHD component ($k_\perp \rho_s \sim 0.1$, in this case corresponding to toroidal mode numbers circa 10 to 15). This component, which does not produce the dominant linear modes, ultimately represents the peak of the spectrum of all the ExB transport channels: particle, and electron and ion heat fluxes. In the scaling, it causes a strong increase of the fluxes (all three channels always scale together in edge turbulence) with beta at values well below the traditional MHD limit, which has no counterpart in the linear growth rates (Fig. 3, lower left). Comparisons of the flux scalings with and without magnetic trapping (variation of B in H_0) in delta-FEFI and also to the GEM results shows all three models show similar trends, with trapping accounting for an ehnacement which is strongest at lowest beta (Fig. 3, upper left). The conclusion of such a result is that linear instability modelling is not a useful guide for tokamak edge phenomenology.

4. Edge Turbulence Gyrofluid Studies

Investigations of a ELM scenario involving a large ideal MHD instability are studied. It is found to saturate upon its own self generated turbulence, in a broad spectrum reaching below the ion gyroradius scale. A depiction of the electron density at the moment of peak flux is shown in Fig. 4. Model geometries for an X-point region are developed. Global self consistency, in terms of the time dependent parallel current determining the magnetic structure, is the new theme. This is required to treat the divertor region with the abovementioned Alfvén oscillation. Geodesic acoustic oscillations (GAM) have been studied with GEM and within a simpler 4-field fluid model. We will present results on parameter dependence of GAMs in the presence of ergodic fields. This work is being published elsewhere.

References

[1] JOLLIET, S. et al., Comput. Phys. Comm. (2007) 409.
[2] PARKER, S. E. et al., Phys. Fluids B **5** (1993) 77.
[3] HAHM, T. S., Phys. Fluids **31** (1988) 2670.
[4] SUGAMA, H., Phys. Plasmas **7** (2000) 466.
[5] FALCHETTO, G. L. et al., Plasma Phys. Contr. Fusion **50** (2008) to appear Oct 08.
[6] WATANABE, T.-H. et al., Nucl. Fusion **46** (2006) 24.
[7] KROMMES, J. A. et al., Phys. Plasmas **1** (1994) 3211.
[8] SCOTT, B., New J. Phys. **4** (2002) 52.
[9] DANNERT, T. et al., Comput. Phys. Comm. **163** (2004) 67.
[10] CANDY, J. et al., Phys. Plasmas **13** (2006) 032310.
[11] KROMMES, J. A., Phys. Plasmas **6** (1999) 1477.
[12] MCMILLAN, B. F. et al., Phys. Plasmas **15** (2008) 052308.
[13] ROSENBLUTH, M. N. et al., Phys. Rev. Lett. **80** (1998) 724.
[14] HIRSHMAN, S. P. et al., Phys. Fluids **20** (1977) 418.
[15] TALA, T. et al., Plasma Phys. Contr. Fusion **49** (2007) B291.
[16] SCOTT, B., Phys. Plasmas **12** (2005) 102307.
[17] SCOTT, B., Phys. Plasmas **8** (2001) 447.
[18] SCOTT, B., Contrib. Plasma Phys. **46** (2006) 714.
[19] SCOTT, B., Phys. Plasmas **12** (2005) 082305.
[20] HAHM, T. S. et al., Phys. Fluids **31** (1988) 1940.
[21] BRIZARD, A., Phys. Plasmas **7** (2000) 4816.
[22] BRIZARD, A. et al., Rev. Mod. Phys. **79** (2007) 421.
[23] HATZKY, R. et al., Phys. Plasmas **9** (2002) 898.
[24] SCOTT, B., Plasma Phys. Contr. Fusion **39** (1997) 1635.
[25] SCOTT, B., Phys. Plasmas **7** (2000) 1845.
[26] NAULIN, V., Phys. Plasmas **10** (2003) 4016.
[27] SCOTT, B., Derivation via free energy conservation constraints of gyrofluid equations with finite-gyroradius electromagnetic nonlinearities, submitted to Phys Plasmas, arXiv:0710.4899, 2007.
[28] BEER, M. et al., Phys. Plasmas **2** (1995) 2687.
[29] SCOTT, B., Phys. Plasmas **5** (1998) 2334.
[30] SCOTT, B., Phys. Plasmas **12** (2005) 062314.
[31] CAMARGO, S. et al., **2** (1995) 48.

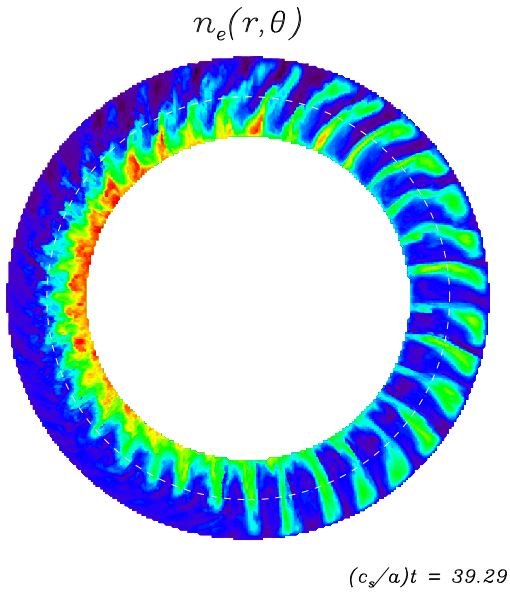

Fig 4. Initial blowout phase of an ELM crash scenario just as the spectrum broadens out to $k_\perp \rho_i > 1$, using GEM.